PERGAMON

International Journal of Heat and Mass Transfer 41 (1998) 2827–2836

International Journal of HEAT and MASS TRANSFER

Flow and mass transfer measurements for a flat plate of finite thickness in pulsating flow

Kwon Sang Hwang, Hyung Jin Sung, Jae Min Hyun*

Department of Mechanical Engineering, Korea Advanced Institute of Science and Technology, 371-1 Kusong-dong, Yusong-gu, Taejon 305-701, South Korea

Received 25 April 1997

Abstract

Laboratory measurements were made of flow and mass transfer over a blunt flat plate of finite thickness, which is placed in a pulsating free stream, $U_\infty = U_0(1 + A_0 \cos 2\pi f_p t)$. Low turbulence-intensity wind tunnel experiments were conducted for small and moderate Reynolds numbers, $770 \leqslant Re_H \leqslant 8000$. Pulsation was generated by means of an acoustic speaker. The majority of experiments were carried out in the ranges of $f_p = 20.0$–80.0 Hz and $A_0 \leqslant 0.15$. Flow properties were measured by I-type and split-film probes. Mass transfer rates were measured by employing the naphthalene sublimation technique. The present results for non-pulsation flows ($A_0 = 0.0$) were shown to be consistent with the published data. For pulsating approach flows, results are provided for the distributions of the wall static pressure, the longitudinal mean velocity and turbulent intensity, and the Sherwood number, Sh, as a function of the stream-wise distance x^* measured from the leading-edge separation point. As A_0 or f_p increases, the time-mean reattachment length is reduced significantly. This implies that the height and length of the separation bubble shrink simultaneously: the position where C_p is recovered moves upstream, and the minimum value of C_p decreases; the reverse flow is intensified; and a substantial augmentation of turbulent energy is discernible. In the separation bubble, the effect of pulsation on Sh is conspicuous. Sh decreases monotonically from the separation point to the minimum value near the secondary separation point; and Sh increases appreciably with increasing x^*, after passing the secondary separation point to the maximum value at the reattachment point; and afterward, Sh decreases. The secondary separation point and the position where Sh has a maximum move further upstream, as A_0 or f_p increases. At large Re_H, the relative influence of pulsation on Sh weakens.

Nomenclature

A_0 pulsating amplitude
C_p pressure coefficient ($\equiv (p-p_0)/0.5\rho U_0^2$)
f_p pulsating frequency [1/s]
H half thickness of the flat plate [m]
p_0 static pressure of free stream [kg s^{-1}]
Re_H Reynolds number ($Re_H \equiv UH/\nu$)
Re_{2H} Reynolds number ($Re_{2H} \equiv U2H/\nu$)
Sh Sherwood number
u longitudinal fluctuation velocity [m s^{-1}]
$\overline{u^2}$ longitudinal component of turbulent energy [m^2 s^{-2}]
u_{rms} r.m.s. value of fluctuating longitudinal velocity component ($\sqrt{\overline{u^2}}$) [m s^{-1}]
U longitudinal local mean velocity [m s^{-1}]
U_0 free stream mean velocity [m s^{-1}]
U_∞ free stream velocity [m s^{-1}]
x streamwise distance from the separation leading-edge [m]
x^* nondimensional streamwise distance from the leading edge ($\equiv x/H$)
x_R mean reattachment length for pulsating flows [m]
x_{R0} mean reattachment length for non-pulsating flows [m]
x_R^* nondimensional streamwise distance from the leading edge ($\equiv x/x_R$)
y vertical distance from the surface of the plate [m]
y_c the y position where u_{rms} is maximum
y_δ time-mean height of the edge of the separated shear layer ($U/U_{max} = 1.0$)
z spanwise distance from the centerline [m].

* Corresponding author. Tel.: +82-42-869-3012; fax: +82-42-869-3210; e-mail: jmhyun@cais.kaist.ac.kr.

0017-9310/98 $19.00
PII: S0017-9310(98)00044-1

Greek symbols

γ_p forward-flow time fraction
ν kinematic viscosity [$m^2 s^{-1}$]
ρ density of air [$kg m^{-3}$].

1. Introduction

Flow about a blunt-faced body, placed in a uniform stream, has been extensively studied. In particular, as a benchmark configuration, much work has been reported for a two-dimensional, semi-infinite flat plate of finite thickness, which is aligned parallel to a uniform approach stream [1–17].

The canonical flow structure includes a variety of essential dynamical elements (see Fig. 1). The flow separates at the sharp corner of the blunt face, and this separated flow reattaches at a downstream location on the surface of the plate. This forms the well-known pattern of a separation bubble, which is defined as a recirculating region bounded by a separated shear layer and a solid surface. The flow is characterized by rolled-up vortices in the shear layer and their interaction with the surface [7]. Farther downstream of the reattachment, the flow undergoes a region of redevelopment, and the overall flow exhibits extremely complex characteristics afterward.

The extent of the recirculating region was described in the experiments by Lane and Loehrke [8], Ota et al. [11] and by Sasaki and Kiya [16] at low and moderate Reynolds numbers. It was found that the steady, laminar separation bubble on the plate grows in size with increasing Reynolds number. The maximum reattachment length was observed at $Re_{2H} \cong 325$, at which oscillations begin in the separated shear layer. As the Reynolds number increases further, the separated shear layer becomes unsteady and the bubble shrinks in size. For large Reynolds numbers, the flow reattachment occurs at about four or five times the plate thickness downstream from the leading edge, and the phenomenon is largely independent of the Reynolds number [2, 5, 10, 11].

Ota and his colleagues [10–13] measured velocity, pressure and turbulence characteristics in the separated, reattached, and redevelopment regions. One major finding was that the mean flow properties approach a nearly fully developed flow at about 20 plate-thickness downstream from the leading-edge.

The effect of the free stream turbulence intensity was studied experimentally in ref. [1]. It was shown that the free stream turbulence promotes rolling-up of the separated shear layer. The rolled-up large-scale vortices were shed downstream from the separation bubble with a frequency of approximately $0.65\, U_0/x_{RO}$ [2, 5–7]. The knowledge on rolled-up vortices is useful in analyzing the turbulence properties, especially in the reattachment region.

Recently, attempts have been made to exert a control on the separated and reattaching flows by introducing localized periodic disturbances immediately behind the separation edge [18, 19]. It was learned that, by providing a sinusoidal disturbance at a proper frequency, considerable alterations were achieved in the overall characteristics of the separated and reattaching flows. The particular frequency of disturbance tested was found to be 4–5 times the frequency of shedding of large-scale vortices from the separation bubble. These studies illustrated the significant role played by the large-scale vortices. At the same time, it was demonstrated that the shedding of vortices as well as the global flow features could be controlled to a considerable degree by externally-provided localized excitations.

The present study proposes to investigate the separated flow over a blunt-faced body in a more practical and widely-encountered situation. Instead of the localized periodic forcing in the vicinity of the separation edge [18, 19], the present work seeks to control the global flow pattern by utilizing the free stream, which contains a well-

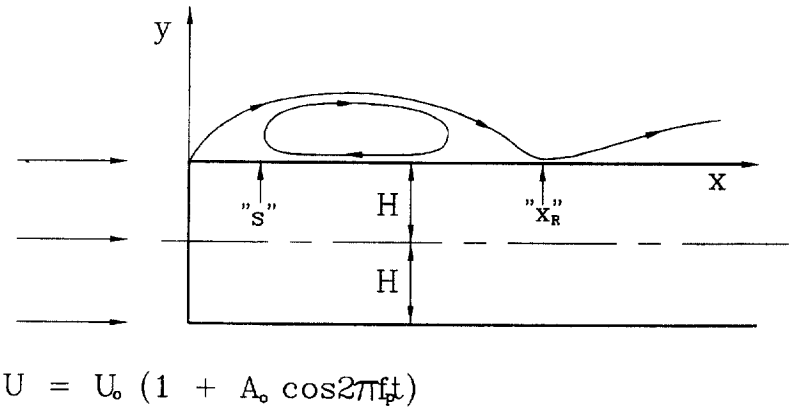

Fig. 1. A schema of flow configurations 's' denotes the secondary separation point and 'x_R' the reattachment point.

defined single-frequency pulsation. The oncoming free stream is expressed as $U_\infty = U_0(1 + A_0 \cos 2\pi f_p t)$. This type of pulsating free stream is in fact a closer representation of some practical engineering problems, such as partially-separated cascade wings and structures exposed to winds. In such applications, inevitable oscillatory components in the approaching free stream, to the lowest approximation, are represented in the above-shown pulsating oncoming flow. The purpose of this study is to depict the impact of free stream pulsation on the formation of the leading-edge separation bubble as well as the shedding of large-scale vortices and on the alterations of transport processes.

A comprehensive and systematically-organized experimental program has been executed. Emphasis is placed on documenting the flow and mass transfer features at moderate Reynolds numbers, $Re_H = 1000$ and 2000. The pulsation amplitude A_0 and frequency f_p are allowed to vary over broad ranges. The mission is to portray the mean and fluctuating velocity fields, both in the streamwise and cross-stream-wise directions, and the transport properties exemplified by the Sherwood number Sh.

In the present experiments, a specially-designed open-circuit blower-type wind tunnel was constructed. The flows were measured by using hot-wires and split-film sensors. The mass transfer measurements were conducted by employing the naphthalene sublimation technique. These methods have been demonstrated to be effective for a variety of related research subjects [4, 20], and they are variable experimental tools for the problem in hand.

2. Experimental apparatus and procedure

The air speed in the test section (250 × 250 mm), U_0, was in the range of 1.5–12.0 m s^{-1}, and the turbulent intensity of the free stream was less than 0.3% [4, 20]. The flat plate, which was fabricated with acrylic resin, was 12.1 mm thick, 250 mm wide, and 550 mm long. The plate was sufficiently long to prevent the interaction between the separated shear layers emanating from both edges [5–7]. The blockage of the plate was 4.84%, which was small so that the main structure of the flow under investigation would not be affected much by the finiteness of the test section [2]. Also, the aspect ratio was 20, which was large enough to render the flow near the centerline approximately two-dimensional [2, 5–7]. The front face of the flat plate was precision-machined to be oriented perpendicular to the oncoming stream. The location of this face was 450 mm downstream of the inlet of the test section.

The pulsation of the free stream was achieved by placing a speaker in the settling chamber. The sinusoidal signal was produced by using a function generator. This signal was passed through an audio amplifier, and it then was sent to the speaker. It is believed that the method of producing pulsation by acoustic means, as in the present work, leads to a simple and straightforward experimental design. To assess the quality of the pulsation superimposed on the uniform free stream, the power spectrum of the free stream velocity field data obtained by an I-type hot-wire was analyzed previously [20]. Based on extensive surveys of the free stream velocity fields, the oncoming velocity has been found, to a high degree of accuracy, to have a sinusoidal pulsation, i.e., expressible by $U_\infty = U_0(1 + A_0 \cos 2\pi f_p t)$. For the wind-tunnel test rig of the present study, the majority of experiments were carried out in the ranges of $f_p = 20.0$–80.0 Hz, $A_0 \leqslant 0.15$.

The mean velocity distribution was measured by using a standard pitot tube and a micro-manometer. To measure the wall static pressure, a total of 42 pressure taps at the centerline of the upper surface of the plate were drilled. A scannivalve and a micro-manometer with a resolution of 0.013 mm of water column were attached therein. The pressure signal (sampling frequency of 6 Hz) was sent to an IBM-486 personal computer through an A/D converter. A total of 4096 pressure signals at a given location were time-averaged to obtain the local pressure coefficient.

To measure flow properties, the hot-wire technique was utilized with constant temperature anemometers (TSI-IFA 100). The sensing material of I- and X-type probes was a 5 μm, platinum-plated, tungsten wire. A single-wire probe (TSI model 1250) was used to monitor the turbulent intensity as well as the pulsation amplitude and frequency of the free stream. A cross-wire probe (TSI model 1246-T1.5) was deployed to measure the turbulent properties except in the re-circulation region. A split-film probe (TSI model 1288) was utilized to depict the flow characteristics, especially in the re-circulating separation bubble.

To ensure precise measurement positioning, probes were made to move in the x and y directions by a remote-controlled two-dimensional traverse system. The resolution was found to be within 0.025 mm. Accurate positioning of the probe was accomplished by a digital height gauge with a sighting microscope, which had a resolution less than 0.01 mm.

Measurement data of mean velocities, turbulence intensities, and forward-flow time fractions were stored after low-pass filtering at a cut-off frequency of 10 kHz. The frequency response characteristics of the hot-wire probes and the split-film sensors were about 20–30 kHz, and these cut-off frequencies were adequate for the present measurements. The velocity signals were digitized at a rate of 10 kHz by using a digitizer (IFA-200), which was equipped with a 14-bit A/D converter. For each measurement point, 40 960 digitizer data were compiled in a removable hard disk (Syquest media) of a personal computer (IBM-486).

Care was exercised in implementing the naphthalene sublimation technique, which formed the core of mass

transfer experiments. The naphthalene-cast portion of the plate was finished to ensure that it had the same roughness and thickness as the rest of the steel plate. In order to quantify the sublimated naphthalene, an automated data acquisition system was installed. The components included a depth gauge with a signal conditioner, a digital voltmeter connected to a GPIB interface, a positioning apparatus driven by stepper motors and an IBM-486 personal computer. Prior to each reading, the gauge was allowed a 0.5-s stabilization period. The measurement of the naphthalene surface profile was performed at a constant room-temperature, which would alleviate possible errors caused by natural convection.

The span-wise variations of mass transfer properties were checked, and they were monitored to be within 1.0%. However, to increase accuracy, measurements were taken at nine span-wise locations ($z/H = 0.0, \pm 0.5, \pm 1.0, \pm 1.5, \pm 2.0$) and they were averaged out at each stream-wise position.

The derivation of the non-dimensional mass transfer coefficient, Sherwood number (Sh), and the full implications of this method have been thoroughly explained in the preceding publications [4, 20].

3. Results and discussion

3.1. Flow characteristics

Figure 2 illustrates the general behavior of the mean reattachment length, x_R, vs. the Reynolds number, Re_H, together with the results of Ota et al. [11] and Kottke et al. [17]. In the present experiments, the time-mean reattachment length, x_R, is defined as the position where the forward time fraction (γ_p) is 0.5. In refs. [11, 17], however, x_R was defined as the distance from the separation point to the point of maximum mass transfer. The range of Re_H covered in the present study belongs to the regime in which the flow separates as a laminar flow, undergoes transition to a turbulent flow, and reattaches as a turbulent flow [2]. The reattachment length, x_R, decreases rapidly with Re_H for relatively small Re_H, and x_R reaches a minimum around $Re_H \cong 2000$. As Re_H increases further, x_R increases mildly. As noted, the previous investigations [8, 11, 16, 17] established the above findings, and it has been observed that the dependence of x_R on Re_H weakens at large Re_H, say $Re_H > 5000$. The apparent minor quantitative disparities between the present results and the preceding reports are thought to be associated with different methods to determine x_R, plate lengths, blockage ratios, aspect ratios, and free stream turbulent intensity. The influence of the blockage and of the aspect ratio of the plate were examined by Cherry et al. [2]. For the present experimental setup [blockage 4.84%, aspect ratio 20.0], the preceding data of [2] give $x_R \cong 10$ H as the large-Re_H limit, which is in good agreement with the present experimental results.

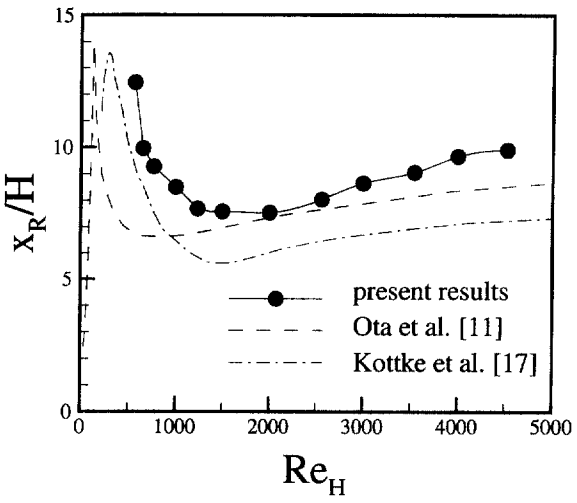

Fig. 2. Time-mean reattachment length x_R vs. Re_H for non-pulsating flows ($A_0 = 0$).

The alterations in x_R brought forth by the introduction of pulsation are exemplified in Fig. 3. Here, the data for $A_0 = 0$ or $f_p = 0$ represent the cases of non-pulsating flow. It is immediately clear that, for the three pulsation frequencies tested, the mean reattachment length decreases as the pulsation amplitude A_0 increases. Furthermore, this trend is more conspicuous for higher pulsation frequencies. Also, for fixed A_0, x_R decreases as f_p increases. In summary, the reattachment length is reduced significantly as a large-amplitude, high-frequency pulsation is added to the free stream. This finding is similar to the results obtained by Parker and Welsh [14] and Hourigan et al. [15] who investigated the effects of transverse perturbation on the flow separation and heat transfer around a blunt plate.

The distribution of pressure on the surface of the plate, expressed in C_p, is displayed in Fig. 4. The data for $A_0 = 0$ corresponds to the case of a non-pulsating free stream, and the C_p-data for this case is consistent with the published results [2, 5]. As exhibited in Fig. 4, the location of minimum-C_p moves upstream, as the pulsation amplitude increases for fixed f_p, or as the pulsation frequency f_p increases for fixed A_0. This implies that the separation bubble undergoes a significant shrinkage in size by the introduction of pulsation. Furthermore, the minimum C_p takes a larger negative value as A_0 increases. This reflects the fact that the reverse flow intensifies, as the impact of the pulsation becomes noticeable. The overall size of the separation bubble is determined basically from a balance between the entrainment rate from the recirculation zone into the shear layer and the re-injection rate from the reattaching shear layer [1]. The pulsation in the free stream is believed to augment the entrainment rate, which

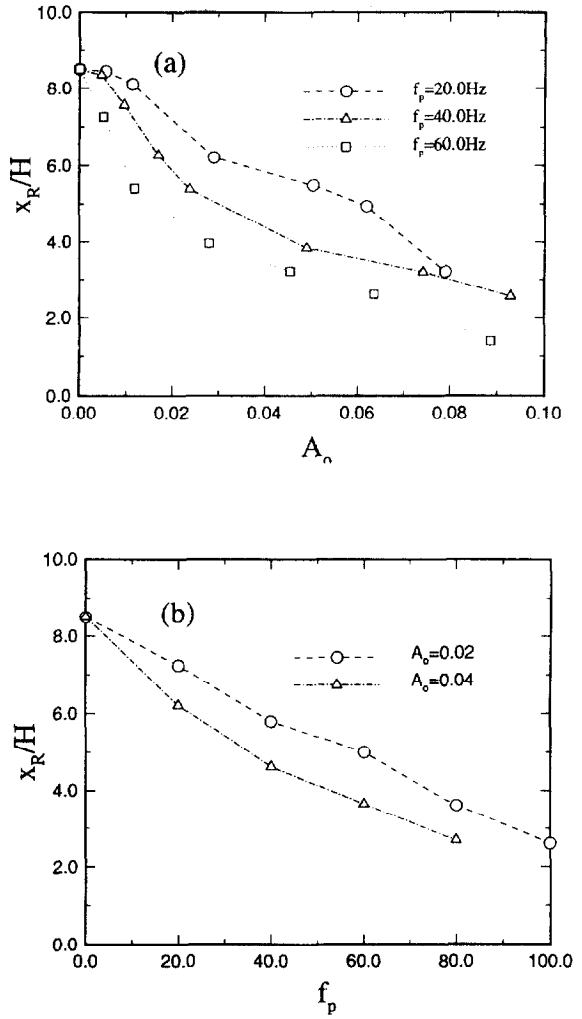

Fig. 3. Variations in time-mean reattachment length x_R for pulsating flows. $Re_H = 1000$. (a) x_R vs. A_0; (b) x_R vs. f_p.

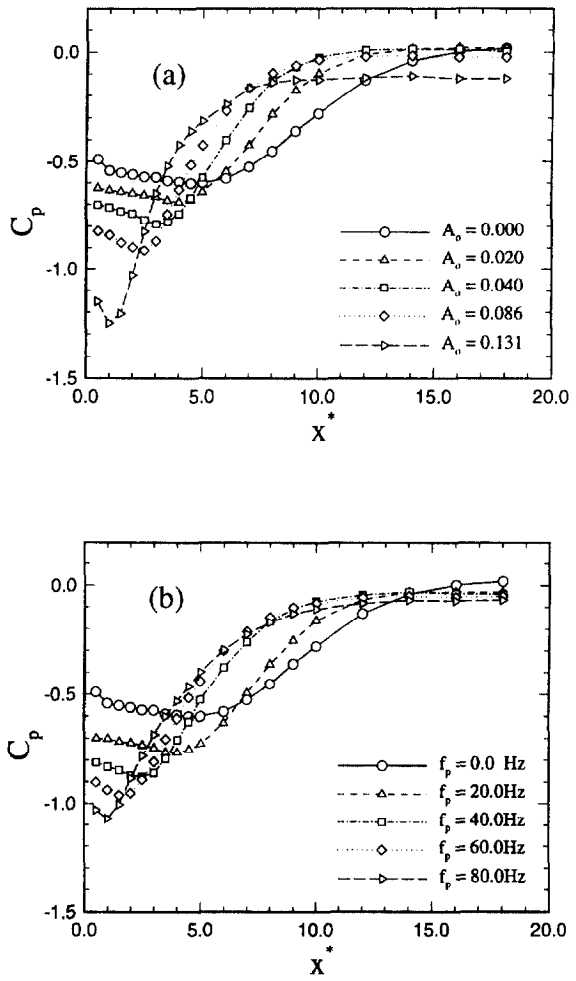

Fig. 4. Stream-wise variations of mean surface pressure coefficient, C_p. $Re_H = 2000$. (a) Effect of A_0 is shown. $f_p = 30$ Hz. (b) Effect of f_p is shown. $A_0 = 0.02$.

turns up in the reduction of the height and length of the separation bubble. Similar results were noted as to the effect of free-stream turbulence on the size of the separation bubble [1]. In related studies, similar findings were obtained for the case of local forcing to the flat front face of an axisymmetric circular cylinder [18, 19].

Another important observation in Fig. 4 is that, with the introduction of pulsation, the pressure at far downstream location ($x \cong 20H$) does not recover its free-stream value. This pressure loss becomes more pronounced as A_0 or f_p increases. The above finding is akin to the effect of free stream turbulence on the separation bubble [1]. This significant non-recovery of pressure at far downstream after the flow reattachment, which is caused by the free stream pulsation, points to the presence of a large-scale vortex. For a pulsating free stream, this large-scale vortex, which sheds from the separation bubble, persists even after the flow has reattached on the surface of the plate. In the case of a non-pulsating free stream, the previous studies indicate that the large-scale vortex shed from the separation bubble weakens through viscous diffusion by its interaction with the wall surface [7]. Consequently, for a non-pulsating flow, a nearly-full recovery of pressure is achieved after the reattachment point [7].

The effect of the amplitude of free stream pulsation, with fixed values of f_p and Re_H ($f_p = 20$ Hz, and $Re_H = 1000$), on the profiles of the mean longitudinal velocity is elaborated in Fig. 5. The measurement points in the longitudinal direction are made non-dimensional by using the reattachment length x_{R0} for the corresponding non-pulsating flow. For the non-pulsating flow, the maximum negative velocity is seen to be $-0.25U_0$ around $x/x_{R0} = 0.6$, which compares favorably

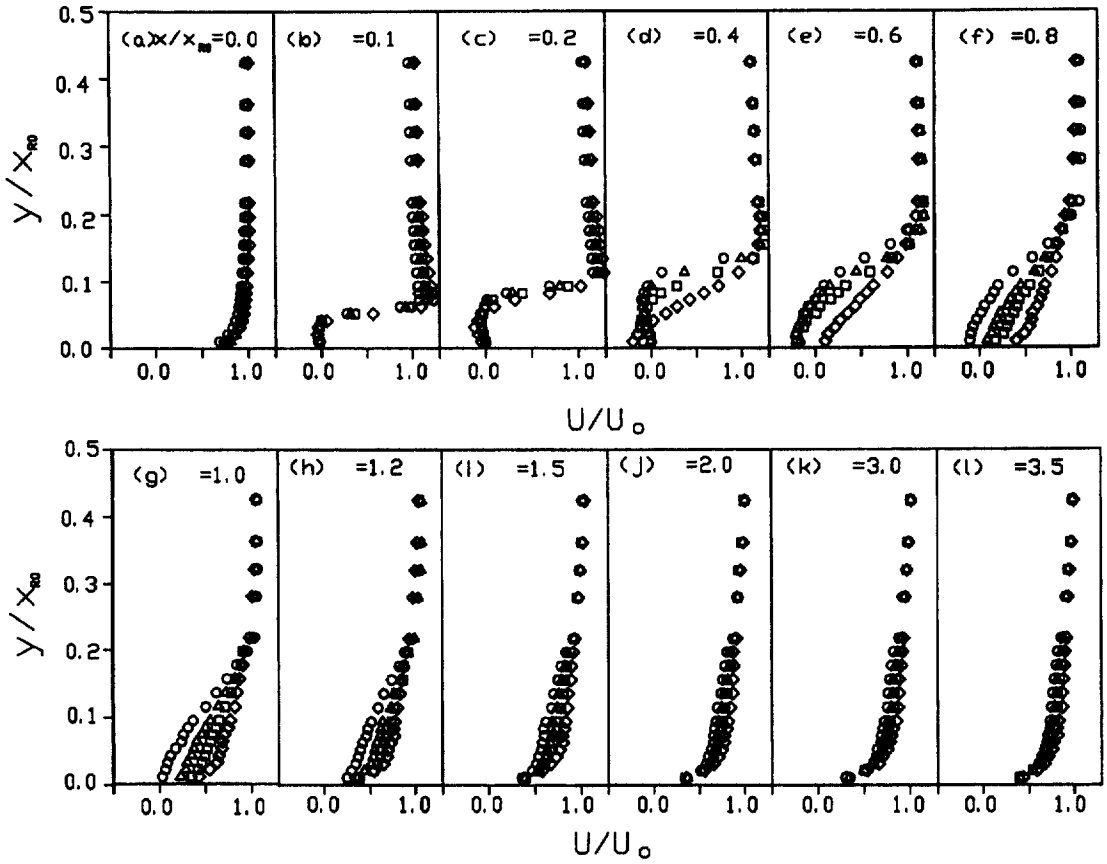

Fig. 5. Stream-wise variations of longitudinal mean velocity U. $Re_H = 1000$, $f_p = 20$ Hz. Symbols indicate: ○, $A_0 = 0$ ($x_R = 8.73H$); △, $A_0 = 0.021$ ($8.08H$); □, $A_0 = 0.059$ ($5.58H$); ◇, $A_0 = 0.082$ ($3.73H$).

with the preceding results for high Reynolds numbers [5, 6]. As pointed out earlier, the introduction of pulsation causes the size of the separation bubble to shrink, both in length and height. Figure 5 also indicates that the impact of pulsation is comparatively weak in the forward portions of the bubble ($x/x_{R0} \leqslant 0.4$); however, the influence of pulsation is relatively strong at farther downstream locations. At still further downstream points, the effect of pulsation weakens, and this is attributable to the increasing viscous effects stemming from the bounding wall. Around $x/x_{R0} > 4.0$, the effect of pulsation on the mean velocity profile appears to have diminished.

Figure 6 exhibits the measurements of velocity profiles by means of a split-film probe. In this case, the pulsation frequency is varied for fixed $A_0 = 0.04$ and $Re_H = 1000$. The longitudinal position x is made dimensionless by using the reattachment length x_R pertinent to each pulsating condition. The lateral position is non-dimensionalized as y/x_{R0}. As stated, as f_p increases, the separation bubble becomes thinner and the reverse-flow intensifies. It is noticeable that, in the forward portion of the plate between the leading-edge separation point and the reattachment point, the reverse flow, in general, weakens measurably due to the viscous effects of the wall. This implies that, by the introduction of pulsation, the point at which the reverse flow becomes zero moves upstream toward the leading-edge. This observation is linked to the behavior of local mass transfer under pulsating conditions, which will be discussed later (see Fig. 11). Obviously, after the reattachment point is passed, the effect of pulsation on the velocity profiles substantially diminishes.

Figure 7 shows the replotted velocity profiles of Fig. 6 in the separation bubble by using y/y_δ and x/x_R. The separation bubbles are seen to collapse nearly into a single separation bubble. This implies that the basic shape of the separation bubble does not change much by the free stream pulsation components. Also, the principal

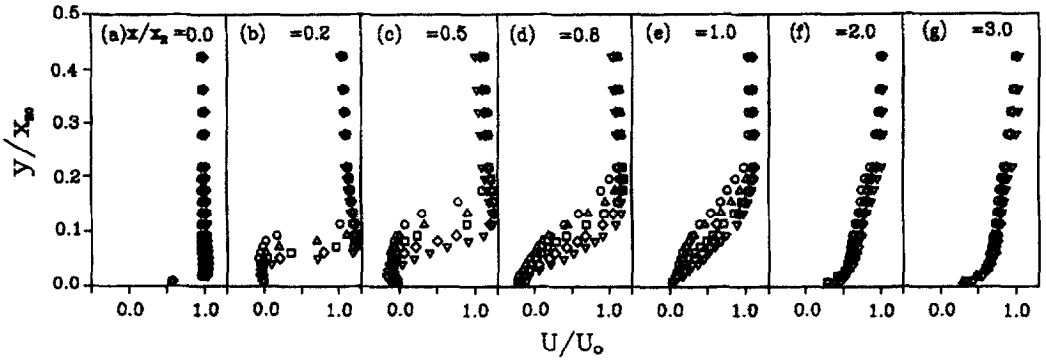

Fig. 6. Effect of f_p on stream-wise variations of longitudinal mean velocity U. $Re_H = 1000$, $A_0 = 0.040$. Symbols indicate: ○, non-pulsating flow ($x_R = 8.73H$); △, $f_p = 20.0$ Hz ($6.21H$); □, $f_p = 40$ Hz ($4.62H$); ◇, $f_p = 60$ Hz ($3.65H$); ▽, $f_p = 80$ Hz ($2.69H$).

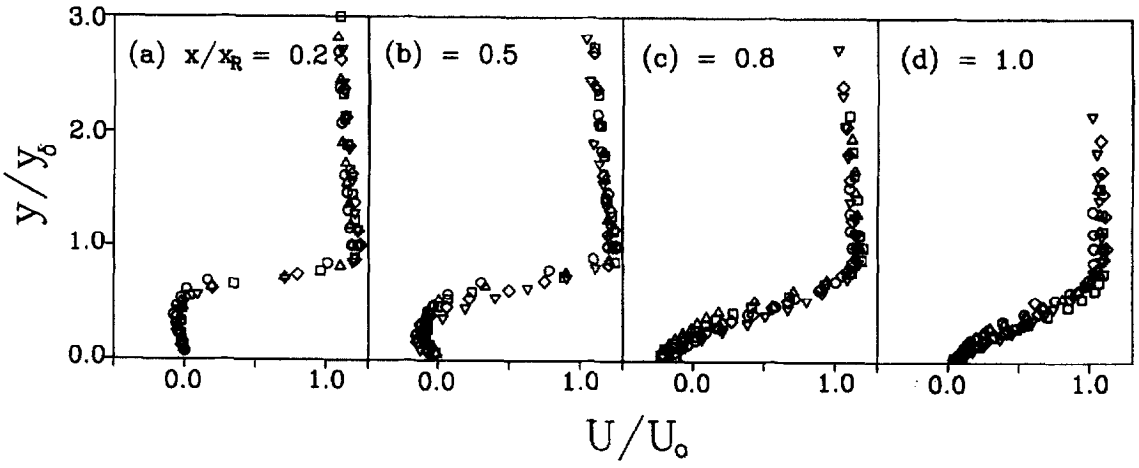

Fig. 7. Enlarged plots of U/U_0 profiles of Fig. 6 in the separation bubble. $Re_H = 1000$, $A_0 = 0.040$. The locations are non-dimensionalized as x/x_R and y/y_δ. Symbols are the same as in Fig. 6.

characteristic length scales for the global configuration of the separation bubble are the time mean reattachment length, x_R and the time-mean height of the edge of the separated shear layer, y_δ. These observations are consistent with the previous report [5].

The turbulent components of velocity are examined in Figs. 8–10. Reference [5] defines the lateral position y_0 at which $\overline{u^2}$ attains a maximum to be the center of the shear layer. This assertion can be verified by cross-comparing the profiles of longitudinal velocity with the distributions of $\overline{u^2}$. For the case of a non-pulsating flow, the value of y_0 varies little with x in the region $x/x_{R0} > 0.6$, which agrees with the previous findings [5]. Also, for the non-pulsating flow, the maximum value of $\sqrt{\overline{u^2}}/U_0$ for $x/x_{R0} > 0.6$ is approximately 0.26, which is in fair agreement with the existing data [5, 6]. After the reattachment point is passed, a sharp decline in the longitudinal normal Reynolds stress, or the longitudinal r.m.s. velocity, is discernible. This is attributable to the presence of the bounding wall in the reattached flow, which leads to inhibition of vortex-pairing process [22, 23].

It is notable that the pulsation gives rise to an appreciable increase of $\overline{u^2}$, and this is most pronounced for $A_0 = 0.082$ at $x/x_{R0} = 0.2$ [see Fig. 8(c)]. A plausible physical explanation is that $x/x_{R0} = 0.2$ corresponds to the location at which the vortex-merging, due to the pulsation component, takes place. It has been ascertained [21] that vortex-pairing increases turbulence intensities in the separated layer; afterward, the turbulence intensity decreases. The gradual attenuation of turbulence intensity is caused by the interaction of the separated shear layer with the bounding wall, and the interaction point is strongly influenced by pulsating components. The present data on $\overline{u^2}$ reveal that, by the introduction of pulsation, the vortex-pairing process is forced to take place in the more forward portion of the plate. This

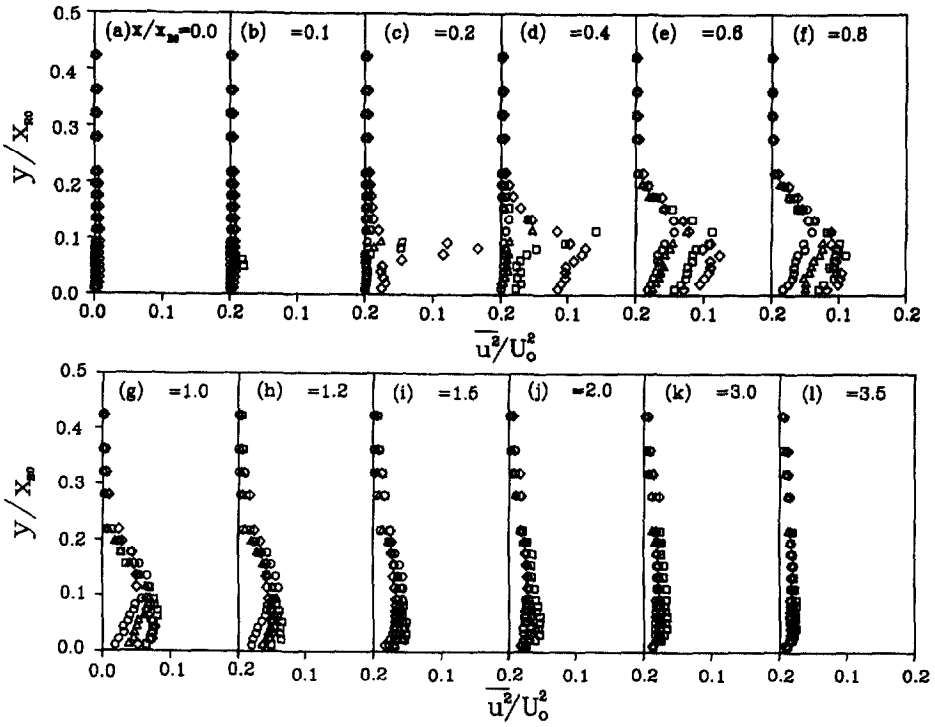

Fig. 8. Stream-wise variations of the longitudinal Reynolds stress u^2/U_0^2. $Re_H = 1000$, $f_p = 20.0$ Hz. Symbols indicate: ○, $A_0 = 0$ ($x_R = 8.73H$); △, $A_0 = 0.021$ ($8.08H$); □, $A_0 = 0.059$ ($5.58H$); ◇, $A_0 = 0.082$ ($3.73H$).

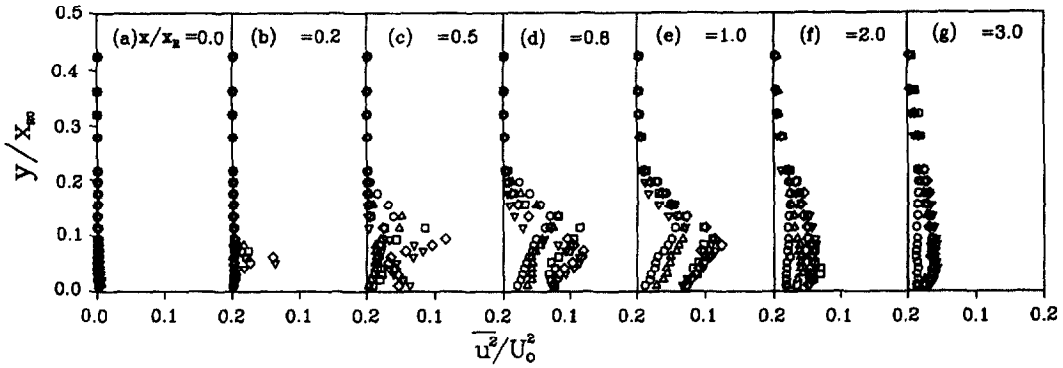

Fig. 9. Stream-wise variations of the longitudinal Reynolds stress u^2/U_0^2. $Re_H = 1000$, $A_0 = 0.040$. Symbols indicate: ○, $f_p = 0.0$ Hz ($x_R = 8.73H$); △, $f_p = 20.0$ Hz ($6.21H$); □, $f_p = 40$ Hz ($4.62H$); ◇, $f_p = 60$ Hz ($3.65H$); ▽, $f_p = 80$ Hz ($2.69H$).

observation runs parallel with the fact that the length of the separation bubble decreases, as A_0 increases.

3.2. Mass transfer characteristics

The measured mass transfer rate, expressed by the local Sherwood number, Sh, is plotted vs. the longitudinal distance x^* ($\equiv x/H$) for varying A_0 in Fig. 11. The earlier studies [4, 9, 10, 13–15] established that the mass (or heat) transfer coefficient attains a maximum around the reattachment point, and decreases monotonically with x^* after this reattachment point. The overall pattern of the Sh-x^* plots fits the above general description. A closer inspection of the plots of Fig. 11 indicates that, for f_p fixed, as A_0 increases, the location of the maximum Sh moves upstream. This is compatible with the observation that the size of the separation bubble is reduced. Also, this trend is corroborative of the distributions of wall static pressure (see Fig. 4) as well as of the mean longitudinal velocity (see Figs. 8–10). With increasing A_0, the

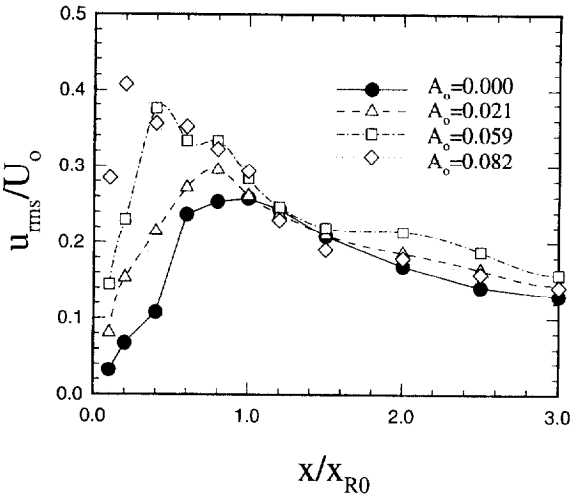

Fig. 10. Stream-wise variations of the maximum longitudinal root-mean-square velocity. $Re_H = 1000$, $f_p = 20.0$ Hz. Symbols indicate: ○, $A_0 = 0$ ($x_R = 8.73H$); △, $A_0 = 0.021$ ($8.08H$); □, $A_0 = 0.059$ ($5.58H$); ◇, $A_0 = 0.082$ ($3.73H$).

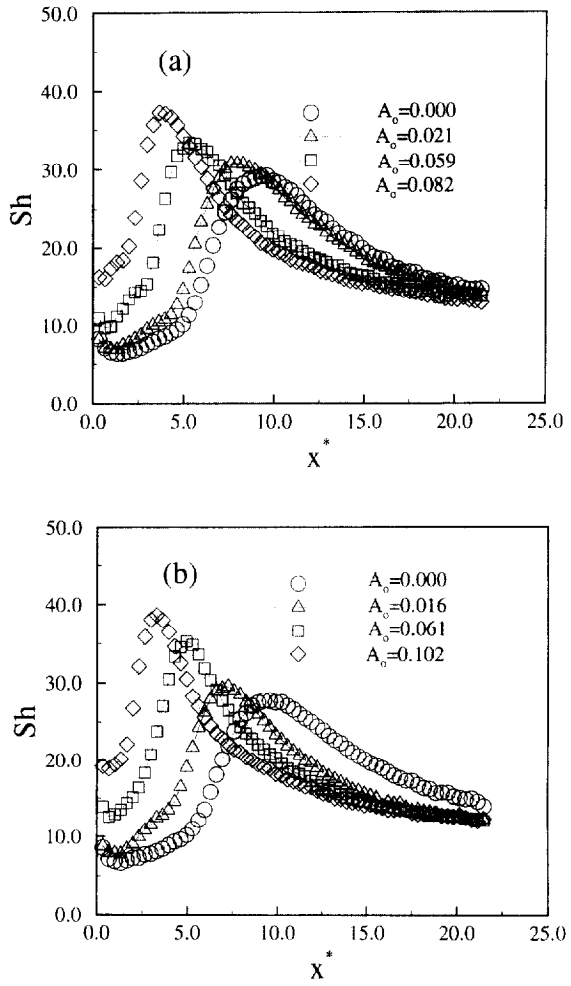

Fig. 11. Stream-wise variations of the Sherwood number Sh. $Re_H = 1000$. (a) $f_p = 20$ Hz, (b) $f_p = 30$ Hz.

augmentation of Sh within the region of the separation bubble becomes discernible. The enhancement of Sh is more pronounced in the forward portion leading to the reattachment point. After the reattachment point is passed, Sh decreases faster with x^* as A_0 increases. Physically, as the pulsation effect increases, the entrainment of the high-energy fluid outside of the separation bubble becomes more vigorous by the action of the intensified re-circulating flow driven by the motion of a large-scale vortex. This causes a substantial augmentation of mass transfer, especially in the vicinity of the reattachment point, which was also observed in the study of Hourigan et al. [15]. They demonstrated that the large-scale vortex structure plays an important role in the transport of energy in the flow. It was also shown that when a transverse sound field is applied, the maximum Nusselt number increases and the location at which this maximum is found shifts toward the leading edge. The Sh-data of Fig. 11 also suggest that the impact of pulsation is far-reaching, well into the far downstream regions ($x/H > 20.0$ in Fig. 11).

In summary, the overall convective mass transfer rate is found to increase when the free-stream pulsation is imposed. It is worth pointing out that this finding is analogous to the case of heat transfer [14, 15].

It is to be mentioned that a local minimum in the Sh-curve is seen in the fore-portion of the plate [e.g., $x/H \cong 1.5$ in Fig. 11(a)]. The existence of this local minimum-Sh was also noted in the previous studies for non-pulsating flows [4]. It was thought that this minimum-Sh point corresponds to the location of the secondary separation point [4, 7] at which the surface velocities are very small (see Figs. 5 and 6). The present results illustrate that, as A_0 increases, the secondary separation point is shifted upstream, due to the strengthened reverse flow. Figure 11 implies that, for the largest value used in the experiment, $A_0 = 0.082$, this secondary separation point has moved upstream such that it nearly coincides with the leading-edge separation point. The influences of f_p, with the same A_0 and Re_H, are evident in Figs. 11(a) and (b). The changes caused by pulsation are more pronounced for higher f_p, and the reduction in size of the separation bubble is more apparent. Figure 12 exhibits the effect of Re_H. At higher Re_H, the changes in the Sh-curves are less pronounced, since the relative influence of pulsation weakens at much higher Re_H.

4. Conclusion

Laboratory experiments were performed to portray the flow and mass transfer characteristics.

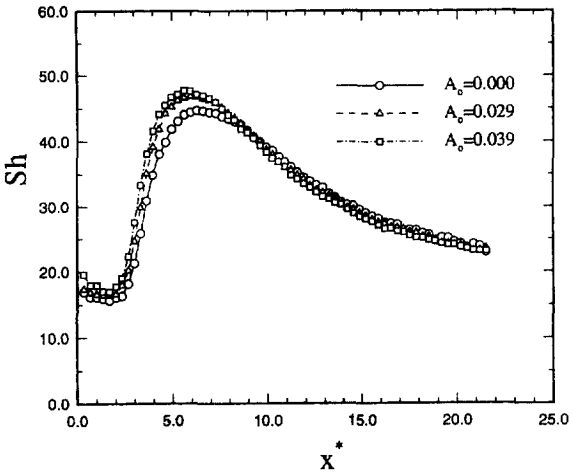

Fig. 12. Stream-wise variations of the Sherwood number Sh. $Re_H = 2000, f_p = 20$ Hz.

By the introduction of pulsating components into the free stream, principal changes in flow characteristics are visible. The reattachment length is reduced measurably, and the separation bubble shrinks in size. The far-downstream pressure does not recover its free stream value. The influence of pulsation is relatively strong in the rearward portion of the bubble. After the reattachment point is passed, the effect of pulsation on the mean velocity profiles diminishes. Also, the pulsation causes an appreciable augmentation of $\overline{u^2}$.

The general pattern of Sh vs. x^* plots indicates that Sh reaches a maximum around the reattachment point. The location of maximum-Sh is shifted upstream as the pulsation amplitude A_0 increases. The enhancement of Sh in the separation bubble is noticeable as the pulsation increases. The alterations brought forth to the Sh–x^* curves are more notable for higher f_p. The comparative influence of pulsation weakens at much higher Re_H.

Acknowledgements

The authors are grateful to the referees who provided constructive comments and additional references. This work was partially supported by a research grant from the Korea Science and Engineering Foundation (KOSEF).

References

[1] Hillier R, Cherry NJ. The effects of stream turbulence on separation bubbles. J Wind Eng and Industrial Aerodynamics 1981;8:49–58.
[2] Cherry NJ, Hillier R, Latour MEMP. Unsteady measurements in a separated and reattaching flow. J Fluid Mech 1984;144:13–46.
[3] Cooper PI, Sheridan JC, Flood GJ. The effect of sound on forced convection over a flat plate. Int J Heat Fluid Flow 1986;7:61–8.
[4] Hwang KS, Sung HJ, Hyun JM. Mass transfer measurements from a blunt-faced flat plate in a uniform flow. Int J Heat Fluid Flow 1996;17:179–82.
[5] Kiya M, Sasaki K. Structure of turbulent separation bubble. J Fluid Mech 1983;137:83–113.
[6] Kiya M, Sasaki K. Structure of a large-scale vortice and unsteady reverse flow in the reattaching zone of a turbulent separation bubble. J Fluid Mech 1985;154:463–91.
[7] Kiya M. Separation bubbles. Theoretical Applied Mechanics 1989;173–91.
[8] Lane JC, Loehrke RI. Leading edge separation from a blunt plate at low Reynolds number. ASME J Fluids Engineering 1980;102:494–6.
[9] Mori S, Nakagawa H, Tanimoto A, Sakakibara M. Heat and mass transfer with boundary layer flow past a flat plate of finite thickness. Int J of Heat Mass Transfer 1991;34:2899–909.
[10] Ota T, Kon N. Heat transfer in the separated and reattached flow on a blunt flat plate. ASME J of Heat Transfer 1974;459–62.
[11] Ota T, Asano Y, Okawa J. Reattachment length of transition of the separated flow over blunt flat plates. Bulletin of the JSME 1981;24:941–7.
[12] Ota T, Narita M. Turbulence measurements in a separated and reattached flow over a blunt flat plate. ASME J Fluids Engineering 1978;100:224–8.
[13] Ota T, Kon N. Turbulent transfer of momentum and heat in a separated and reattached flow over a blunt flat plate. ASME J Heat Transfer 1980;102:749–54.
[14] Parker R, Welsh MC. Effects of sound on flow separation from blunt flat plates. Int J Heat Fluid Flow 1983;4:113–28.
[15] Hourigan K, Welch LW, Thompson MC, Cooper PI, Welsh MC. Augmented forced convection heat transfer in separated flow around a blunt flat plate. Experimental Thermal and Fluid Science 1991;4:182–91.
[16] Sasaki K, Kiya M. Three-dimensional vortex structure in a leading-edge separation bubble at moderate Reynolds number. ASME J Fluids Engineering 1991;113:405–10.
[17] Kottke, V, Blenke H, Schmidt KG. Einfluss von anstromprofil und turbulenzintensitat auf die unstromung langsangestromter platten endlicher dicke. Warme-und Stoffubertraung 1977;10:159–74.
[18] Sigurdson LW, Roshko A. The structure and control of a turbulent reattaching flow. Turbulence Management and Relaminarisation IUTAM Symposium. Bangalore, India: Springer-Verlag, 1988.
[19] Sigurdson LW. The structure and control of a turbulent reattaching flow. J Fluid Mech 1995;289:139–65.
[20] Sung HJ, Hwang KS, Hyun JM. Experimental study on mass transfer from a circular cylinder in pulsation flow. Int J Heat Mass Transfer 1994;37:2203–10.
[21] Chun KB, Sung HJ. Control of turbulent separated flow over a backward-facing step by local forcing. Exp Fluids 1996;21:417–26.
[22] Troutt TR, Scheelke B, Norman TR. Organized structures in a reattaching separated flow field. J Fluid Mech 1984;143:413–27.
[23] Bhattacharjee S, Scheelke B, Troutt TR. Modification of vortex interactions in a reattaching separated flow. AIAA J 1986;24:623–9.